Experimental Determination and Numerical Evaluation of Core Losses in a 150-kVA Wound-Field Synchronous Machine

P. Rasilo, A. Belahcen, A. Arkkio

Aalto University School of Electrical Engineering, Dept. of Electrical Engineering, P.O. Box 13000, FI-00076 Aalto, Finland

E-mail: paavo.rasilo@aalto.fi

Abstract

The losses in the laminated core of a 150-kVA wound-field synchronous machine are investigated with calorimetric measurements and a numerical iron-loss model for steel laminations. Both grid supply and pulse-width modulated inverter supply with 1-kHz and 6-kHz switching frequencies are studied. The effect of rotor lamination material on the total core losses is studied by measuring and simulating the machine with three prototype rotors, the first one being stacked of insulated 0.5-mm Fe-Si sheets and the last two of uninsulated 1-mm and 2-mm steel sheets, respectively. At no load, the losses in the frame of the machine are shown to be extremely significant with voltages above the rated one. The results on load operation show that the additional inverter-induced core losses are significantly larger with the thicker sheets. The rotor eddy-current loss is the most affected component due to the loading and the distorted supply voltage. However, unlike expected and predicted by the model, the differences in the losses between the 1-mm and 2-mm rotors are negligible in no-load operation and relatively small also at load operation.

1. Introduction

Accurate determination of core losses has remained a challenge throughout the history of electrical machines. During the last few decades, this problem has been further complicated by the increasing use of static power converters causing additional losses in the machines. Up to this date, the additional inverter losses have been studied extensively, mostly in either simple test cores [1], [2], or induction machines [3]-[13]. In addition, permanent-magnet machines have been receiving increasing attention during the last decade, mostly due to the losses in the magnets [14], [15].

The challenge in the prediction of iron losses is revealed by the fact that most of the models in [1]-[13] are rather empirical in nature, often based on different modifications of the Steinmetz formula [16] or the statistical loss-separation theory of Bertotti [17], and identified from a large amount of experimental data. Although such models are simple to implement, they fail to properly explain the physical background of the core losses and their increase due to nonsinusoidal supplies. From the reviewed papers, only [6] included a more detailed physical model describing the eddy currents in the core laminations. In addition, although most of the papers [3]-[13] validated the used models by means of measurements on actual machines, the measurement accuracies were not stated. Since the accuracy of electrical power measurements can significantly suffer from the distorted inverter voltage waveforms, the error in the loss measurement can easily become large if the losses are determined as the difference between the input and output powers of the machine. Direct loss measurements by calorimetric methods are known to provide a good accuracy independent of the supply [18].

Compared to induction machines, the losses in wound-field synchronous machines (WFSM), have been studied much less. Owing to the synchronous operation, their fundamental rotor frequency is zero, and thus their rotors are usually either made of solid steel or stacked of thick uninsulated steel sheets in order to reduce manufacturing costs. The effect of inverter supply on the eddy-current losses in solid poles has been the topic of few reports [19], [20], but so far the laminated poles seem to have been considered rather uninteresting and to be only little influenced by the inverter supply [21]. In fact, however, the use of thick, highly conductive and uninsulated laminations exposes the pole surfaces to high-frequency eddy-currents induced by the

distorted air-gap flux density at inverter supply. Considering the high powers of synchronous machine applications, we find it important to study the effect of the inverter supply on the core losses also in the WFSMs. Possibilities of reducing these losses easily lead to large absolute energy savings in the drive, as well as in the whole energy conversion and transmission chain.

In this paper, we perform a study of the core losses for a 150-kVA, 400-V, 4-pole, laminated-rotor synchronous machine. By core loss, we mean not only the iron loss, but also any other loss component included in the total electromagnetic losses of the machine, but not in the winding copper losses calculated based on DC resistance measurements. A calorimetric measurement system is used to directly determine the total electromagnetic losses with grid supply, as well as with pulse-width modulated (PWM) inverter supply using switching frequencies of both 1 and 6 kHz. From the total electromagnetic losses, the core losses are segregated by subtracting the copper losses of the windings. Three rotors stacked of insulated 0.5-mm Fe-Si sheets and 1-mm and 2-mm uninsulated steel sheets are used in the measurements. The calorimetric method yields good enough accuracy in order to properly distinguish the effect of rotor lamination material on the losses. It is shown experimentally that the 1-mm and 2-mm laminations are much more severely influenced by the loading and the distorted voltage waveform than the 0.5-mm sheets.

We also contribute to the field of numerical evaluation of the core losses by modeling the test machine with the 2-D finite-element (FE) method coupled to models for the hysteresis, eddy-current and excess losses in the core laminations. The aim is to segregate the losses into different components as well as to evaluate the suitability of the FE model and the lamination model to predict the total core losses. Contrary to the most commonly-used experimental iron-loss models, the applied model is more physical in nature which makes it valid for arbitrary and distorted flux-density waveforms and allows its identification from a smaller amount of experimental data. Only the static major hysteresis loops and the electrical conductivities are needed for the sheets.

2. Methods

2.1. Test Machine

The test machine is a 150-kVA low-voltage synchronous generator for an industrial diesel-generator application. The rated data and some dimensions of the machine are summarized in Table I. The stator slots of the machine have been axially skewed by one slot pitch to reduce the harmonic contents of the no-load voltage.

For the test machine, three rotors identical in geometry but stacked of different lamination materials were manufactured in order to study the dependency of the losses on the sheet material and to verify the lamination model. The first rotor is stacked of insulated 0.5-mm Fe-Si electrical steels while the last two are stacked of 1-mm and 2-mm uninsulated steel sheets, respectively. The electrical conductivities of the materials are summarized in Table II. The stator material is the 0.5-mm Fe-Si sheet used for the first rotor.

2.2. Calorimetric Measurement System

The measurements were performed with the calorimetric system described in detail in [25]. The total losses were determined from the heat dissipation of the machine by measuring the temperature rise, mass flow rate and heat capacity of the cooling air. To calibrate the system, the power transferred by the coolant air was first measured as a function of DC power supplied to heater resistors. During the actual test run, the machine losses were then obtained from the calibration curve by interpolating to the measured coolant power. This comparison allows any heat leakage or systematic measurement errors to be neglected from the results, provided that the thermal conditions between the calibration measurement and the test run are identical. To obtain direct correspondence between the heater power and the total electromagnetic losses, the unexcited test machine was rotated by a prime mover during the calibration.

The measurement error has been estimated theoretically by calculating the combined uncertainty in the power loss based on the inaccuracies of the sensors and the differences in the heat-leakage conditions between the test run and the calibration. Errors of 5.0 %, 2.9 % and 1.9 % were reported in [25] for the total electromagnetic losses at no-load operation, and at 50 % and 100 % loads, respectively. From the total electromagnetic losses, the core losses are segregated by subtracting the copper losses of the armature and field windings. In addition to the iron losses, the core losses will thus include, for instance, the losses caused by the damper-winding currents, circulating currents in the parallel conductors of the stator winding as well as eddy currents and hysteresis in the frame and other support structures of the machine.

2.3. Finite-Element Model with Lamination Iron Losses

The core losses are numerically analyzed with the 2-D FE method including a model for the core lamination iron losses [26]. In brief, the model couples the 2-D FE solution of the flux-density distribution in the cross section of an electrical machine to a numerical solution of the 1-D diffusion problem for the flux density in the core lamination. If the cross section is placed in the *xy*-plane, the *z*-axis points in the axial direction and the 1-D problem is described by

$$\frac{\partial^2 \boldsymbol{h}(z,t)}{\partial z^2} = \sigma \frac{\partial \boldsymbol{b}(z,t)}{\partial t} . \tag{1}$$

Here $\boldsymbol{h}$ is the magnetic field strength, $\boldsymbol{b}$ is the magnetic flux density and σ is the electrical conductivity of the lamination material. The constitutive magnetic material law, i.e. the $\boldsymbol{h}(\boldsymbol{b})$ relationship, is generally hysteretic and possibly rate-dependent if local excess losses are considered. The inverted vector Preisach hysteresis model (PHM), and a dynamic expression for the excess field strength are used to model the hysteretic and rate-dependent magnetization properties. However, to improve the convergence properties and to speed up the computation, only single-valued (SV) material properties are considered during the FE solution, and the hysteresis and excess losses are calculated in the post-processing stage. This can be done without a significant loss of accuracy as justified in [27]. The hysteresis, classical eddy-current and excess losses are calculated from the 1-D flux-density distribution as described in [26].

The mesh of the machine is shown in Fig. 1. To evaluate the losses in the support structures around the core, the steel frame is modeled as a solid conducting region. Since the conductivity and the magnetization properties of the frame are not known accurately, they are assumed to be the same as those of the shaft.

The axial skewing is not taken into account in the 2-D model. Based on the results of [28]-[31], the inter-bar currents flowing between the damper-winding bars are known to be increased by the skewing, which is likely to cause the actual rotor core losses to be larger than the simulated ones. The skewing could be modeled with a sliced 2-D model coupled to a circuit representation of the inter-bar currents [32], but determining a suitable value for the bar-to-iron contact resistance is difficult since the phenomenon is very statistical in nature [30], [31]. Owing to the skewing, the harmonic contents in the measured no-load voltage and armature current are likely to be smaller than in the simulated ones. Thus, the operation points at no-load and load operation were determined from the fundamental component of the no-load voltage and the active electrical power, respectively, for both the simulations and measurements. In addition to the skewing effects, the circulating currents in the parallel paths and wires of the stator winding are neglected from the FE model. For the parallel paths, these currents were measured and noticed to be negligible.

In all of the simulations presented in this paper, 2nd-order FEs were used and one supply period was discretized into 2000 time steps. The rotor was forced to rotate at the synchronous speed while the stator and field windings were supplied from voltage sources, except in open-circuit operation in which the stator current was set to zero. To accurately model the skin effect, (1) was solved by approximating the flux density by a three-term cosine series as seen necessary in [27].

2.4. Identification of Core Materials

One aim of this work was to identify the materials with as few measurements as possible. Thus only the static major hysteresis loops were measured for the three materials, and a theoretical approach was used to determine the Everett functions required for the PHM [33]. The magnetization curves were measured from 300 mm × 30 mm Epstein strips cut in arbitrary directions to neglect any effects of anisotropy. The first-order reversal curves (FORCs) were determined analytically by employing the approach of [34] with the exception that numerical interpolation was used instead of an analytical function to approximate the major loop. In the approach, the FORCs are modeled by a simple analytical function ensuring their intersection at the selected maximum flux density b_s, above which the material is assumed anhysteretic. The notation is shown in Fig. 2 a). The difference Δb in the flux density between the descending major loop (denoted by the h- or b-based functions $b_{\mathrm{maj},-}(h)$ or $h_{\mathrm{maj},-}(b)$) and a descending FORC (determined by the reversal point (h_1^+, b_1^+)) varies according to

$$\Delta b(b) = \left(b_{\mathrm{maj},-}\left(h_1^+\right) - b_1^+\right)\left(\frac{b+b_s}{b_1^+ + b_s}\right)^{1+\beta\frac{|b|}{b_s}}, \tag{2}$$

in which the constant parameter β controls the shape of the FORCs. Knowing Δb, the value of h on the FORC can be determined from the major loop as

$$h(b) = h_{\mathrm{maj},-}\left(b + \Delta b(b)\right). \tag{3}$$

More details on the model can be found in [34].

From the analytical FORCs, the Everett function for the scalar PHM was calculated according to [33]. The vector model, [35], applies the scalar model into a finite number of directions, and sums up the results to form the output field-strength vector. The Everett function for the vector model has to be identified so that the model produces the unidirectionally measured Everett function as output when supplied with alternating flux density. This identification problem derived in [35] was solved by the Gauss-Jacobi integration method presented in [36].

In the numerical implementation, the major loops were discretized into 100 steps equally distributed in b. The same 100 points were used as the reversal points for the FORCs. Due to the lack of experimental FORC data and since the effect of the minor loops on the results of the FE simulations can be considered to be relatively small especially in a saturated machine, parameters β were chosen so that the FORCs output from the vector model seemed visually reasonable and didn't cross the major loop. For the 0.5-mm, 1-mm and 2-mm sheets, respectively, the values of b_s were 2.07 T, 1.603 T, and 1.603 T, and the values of β were 9, 2 and 5. Fig. 2 b) shows the modeled and measured hysteresis loops for the three materials. Some modeled minor loops and the SV curves used in the calculation are also shown. The 0.5-mm Fe-Si sheet can be seen to have a higher permeability below 1 T and much smaller static hysteresis loss than the other two sheets.

To verify that the material properties and the FE model were implemented correctly, the no-load and short-circuit curves were measured and compared to simulations. The open-circuit operation is a good operating point for verifying the material properties while the short-circuit curves can be used to verify that the circuit equations are implemented correctly. A good correspondence in both cases can be observed in Fig. 3 for all the three rotors. The effect of the rotor material on the no-load curve is small since the no-load current is mostly determined by the air-gap length and the relatively long stator back iron.

3. Application and Results

3.1. Losses in No-Load Operation

The no-load core losses were both measured and simulated with open stator terminals as a function of the terminal voltage. The results with the three rotors are shown in Fig. 4, in which the losses measured at 400 V with the 1-mm rotor are indicated by the horizontal line for comparison. The measurement errors are indicated by the error bars, and the simulated core losses are segregated into hysteresis, classical eddy-current and excess losses, damper winding losses and frame losses. Table III shows the numerical values of the losses at certain voltages and segregates the simulated losses into stator and rotor losses. The first remark is that at voltages above the rated one, the frame loss is extremely significant in order to explain the increase in the measured core losses. In the 0.5-mm and 1-mm cases, the frame loss becomes the most significant loss component at voltages above 440 V. For further validation of the frame losses, Fig. 5 a) compares the measured and simulated peak flux-densities in the frame at different voltages with the 1-mm rotor. The measured values were determined by measuring the root-mean-square (rms) voltage of a search coil wound over the frame ring (see Fig. 1), integrating the voltage by assuming a sinusoidal time-variation, and averaging the obtained flux over the 3-mm thickness of the ring. The sinusoidal assumption may explain the differences between the measured and simulated results at higher voltages, when saturation reduces the ratio of the peak and rms values. Either way, the results indicate that the peak flux densities rise close to the range of 0.8-1.0 T at 480 V. The high measured steady-state temperatures shown in Fig. 5 b) also imply significant losses in the frame.

With the 0.5-mm and 1-mm sheets, the measured and simulated core losses compare quite well to each other, the difference at 400 V being 11-13 %. When the rotor sheet is changed from the 0.5-mm sheet to the 1-mm sheet, the measured 400-V losses increase from 1257 W to 1550 W, i.e. by 23 %. A 25 % increase, i.e. very similar behavior, is observed in the simulated losses. In the 0.5-mm case, the most accurate results are obtained at 340 V when the flux densities in the stator yoke and teeth are close to 1.4 T. In this case, the accurate shape of the FORCs is insignificant and the losses in the frame are small. In the simulations with lower voltages, the accurate FORC shapes become more significant, while at higher voltages the losses in the frame start to increase. It can be seen from Table III that the stator losses are negligibly influenced by the rotor material.

The decrease in the hysteresis losses at higher voltages is caused by the saturation of the rotor. The high-frequency flux-density harmonics on the rotor surface are induced over a DC bias component caused by the field current. With high field current values, the rotor iron is saturated and the energy loss related to the minor loops of the high-frequency harmonics decreases.

When the rotor lamination is changed from the 1-mm sheet to the 2-mm sheet, the losses obtained from the lamination model grow approximately in the same proportion as when changing from the 0.5-mm sheet to the 1-mm one. The increase is caused by the rotor eddy-current losses which grow by 150-300 % depending on the voltage. However, the measured losses can surprisingly be seen to remain almost equal to the 1-mm case. This means that the lamination model is unable to describe the actual behavior of the field in the machine. Since the model is based on the assumptions that the core laminations are perfectly insulated from each other, and no currents flow in the stacks in the axial direction, it appears that the uninsulated sheet stacks behave in reality more like solid cores rather than ones with negligible axial eddy currents. Thus in the following, we perform a brief study for the contact resistances between the uninsulated laminations.

3.2. Uninsulated Lamination Stacks

The effect of insulating coating on the interlaminar eddy currents have been discussed quite little earlier in the literature. In [22], increases of only a few percent were observed in the losses of toroids stacked of uninsulated laminations in comparison to ones with a good interlaminar insulation. However, the author of [23] obtained better correspondence between numerically predicted

and measured inductance values of a transformer core stacked of insulated 0.35-mm laminations, when the interlamination effects were included in the model. The authors of [24] reviewed some earlier studies and concluded that the surface resistivity values do not give enough information on the losses, which are actually dependent on the size of the contact surfaces.

Despite the seemingly complex nature of the problem, the average resistivities of stacks of two lamination samples were measured to get some insight on the contacts. The 150 mm × 150 mm samples were overlapped by a width of 40 mm, and 8-mm thick copper bars were placed above and below the overlapping regions to equally distribute the 15-A DC current supplied through the laminations. The voltage over the samples was measured from the copper surfaces closest to the laminations. The whole stack was pressed together with a hydraulic press, and the average resistivities over the stacks were recorded. To exclude the copper-steel contact resistances, the resistance values obtained similarly for a stack of only one lamination were subtracted from the results. Fig. 6 a) shows the resistivities for the two materials as a function of the pressing stress. The resistivities can be seen to approach values of approximately 0.3-0.4 mΩm, corresponding to conductivities of about 2.5-3.3 kS/m. Since the original samples were slightly dusty and oily having been stored for a long time, they were next cleaned first with water and then with a dissolvent capable of removing grease, fingerprints etc. from metal surfaces. The increases in the conductivities due to the cleansing can be seen in Fig. 6 b). The conductivities were noticed to vary significantly when different surfaces of each lamination were pressed together. Thus only the maximum conductivities obtained from a set of several measurements with the highest available pressing stress are shown. For both materials, the conductivities are more than doubled due to the cleansing. However, they are still very small when compared to the values in Table II which means that significant contact resistances still exist between the laminations due to uneven surfaces, oxide layers etc. which agrees with the findings of [22] and [24]. In addition, the results of the resistivity measurements imply that in the actual rotor stacked of hundreds of such laminations, the contacts between the laminations are likely to be very statistical in nature.

If the contact resistances are sufficient to prevent axial eddy currents, another factor that may cause the negligible difference between the losses of the 1-mm and 2-mm rotors is that the 2-mm sheets were cut by wire cutting, while the 1-mm sheets were punched. Punching is known to cause plastic deformations near the edges of the laminations and to deteriorate their magnetic properties, which results in increases in the iron losses. The effects of wire cutting on the magnetic properties have not been studied much in the literature but it is possible that this process has a smaller effect on the losses. Since the rotor losses occur close to the pole surface and thus the cutting edges, it is possible that the losses in the 1-mm sheets are significantly increased due to the punching defects and thus close to the losses of the 2-mm sheets.

3.3. Losses in Loaded Operation

At loaded operation, the losses were measured in the motoring mode of operation with each rotor using grid supply and both 1-kHz and 6-kHz PWM inverter supplies. The rated displacement factor, 0.8 capacitive, was used in all loading points. The core losses at different loads are compared in Fig. 7 and Table III, in which both the measured and simulated losses have been linearly interpolated to the same active powers. The simulation results are shown similarly to the no-load case. The PWM simulations were made both with the measured voltage waveforms and ones obtained from a simple sinus-triangular comparison. Both waveforms were found to yield almost equal losses.

Contrary to the no-load case, the losses increase also when changing from the 1-mm sheet to the 2-mm sheet, at which the measured losses actually compare well with simulated ones. However, this increase is still smaller than that observed when changing from the 0.5-mm sheet to the 1-mm one. From the simulation results shown in Table III it can be seen that again only the rotor losses are significantly affected by the sheet material.

A more detailed numerical segregation of the core losses reveals that the rotor eddy-current loss is the most affected

component due to loading. In fact, the stator eddy-current losses as well as all the other loss components change only negligibly when compared to the rotor eddy-current loss. The difference in the loss distributions between the rated-load and no-load operation are shown in Fig. 8 a) for the 1-mm rotor with 1-kHz PWM supply. The rotor-surface eddy currents grow with loading due to the increased spatial harmonic contents in the air-gap magnetomotive force caused by the stator currents.

The measurement results show that at the rated load, changing from the grid supply to the 6-kHz PWM supply increased the core losses in the 0.5-mm, 1-mm and 2-mm rotors by 19 %, 24 % and 22 %, respectively. Similarly, when decreasing the switching frequency from 6 kHz to 1 kHz, the losses further increased by 12 %, 9.5 % and 19 %. From the simulated values of Table III and the distribution in Fig. 8 b), the additional inverter loss can also be seen to be induced mostly on the rotor side. Similarly to the findings in [37] for a higher-power laminated-core machine and in [20] for a solid-rotor machine, the additional losses are induced mostly on the lagging edge of the pole shoe. This is explained by Fig. 9, which shows the difference in the instantaneous flux-density distributions between the 1-kHz PWM supply and the grid supply. Similarly to [20], the high-frequency flux can be seen to penetrate mostly through the lagging edge of the pole due to the higher permeability than on the saturated leading edge.

With the 0.5-mm and 1-mm rotors, the difference between the measured and simulated results can be seen to increase with the loading. This means that in the real machine, there are some load-dependent loss components not taken into account in the 2-D model. In [28], the rotor pole-face losses in the test machine were analytically predicted to increase by 18 % due to the introduction of the skewing. However, even such an increase wouldn't explain the differences in the 0.5-mm and 1-mm cases where the stator hysteresis and eddy-current losses still comprise most of the core losses. On the other hand, [28] didn't consider the inter-bar currents which according to [30] can be a significant source of stray-load losses at least in skewed induction machines, and thus may also contribute to the difference in this case.

However, when the supply-voltage waveform becomes more distorted, mainly the load-independent differences between the measured and simulated losses increase. Thus it is likely that some eddy currents also occur in the stator and rotor end plates and are maybe also induced in the stack-end laminations by the end-winding fields. These eddy-current losses would naturally increase due to the increased harmonic contents in the voltage and flux and cause the increased difference between the measurements and simulations. Estimation of these losses would require using 3-D FE models.

Considering the aforementioned shortcomings in the 2-D model, the overall correspondence between the simulated and measured results can be considered to be sufficient at least in the case of the 0.5-mm Fe-Si rotor. In the 2-mm case, the results seem to correspond even better, but it is not exactly clear whether this is caused by the FE model overestimating the rotor eddy-current losses similarly to the no-load case while neglecting the other load-dependent loss components, or by increase in the losses of the 0.5-mm and 1-mm rotors due to punching.

4. Conclusion

Core losses in a 150-kVA synchronous machine were studied both experimentally and by numerical simulations. Results with three different rotor lamination materials were presented. Despite the simple identification process for the three materials, a relatively good correspondence was obtained between the simulated and measured core losses.

The losses in the frame significantly increased when voltages above the rated one were used. The simulated frame losses started to increase at 380 V when the yoke flux density exceeded 1.4 T. When the yoke saturates, the solid-steel frame offers an easier path for the flux density, and the losses are increased due to significant eddy currents. For good performance, it should be ensured in the design stage that no excessive losses occur in the frame at the rated voltage. Based on the no-load simulations, the 2-D FE method appears to give sufficient information on the losses in the frame for this purpose. In everyday design tools,

limiting the yoke flux density to a suitable value is likely to prevent the flux from penetrating the frame.

The measurement results imply that using 0.5-mm sheets should be seriously considered when designing synchronous machines for inverter operation. It can be calculated from Table III that the rated-load core losses with grid supply were increased by 66 % when the 2-mm sheet was used instead of the 0.5-mm one. In addition, the 1-mm and 2-mm sheets were much more seriously affected by the frequency-converter supply than the 0.5-mm sheet. However, the differences in the losses between the 1-mm and 2-mm rotors were found to be much smaller than expected and predicted by the FE model. This was concluded to be caused either by the very statistical galvanic contacts between the uninsulated laminations, or the different cutting methods used for the 1-mm and 2-mm sheets.

Based on the simulation results, the rotor eddy-current loss is the most affected loss component due to both the loading and the inverter supply. Thus the total core losses may be reduced by changing the air-gap length and the rotor pole-shoe construction. In [38], a preliminary study showed that significant reductions are possible by relatively simple structural design changes. The modulation technique and the switching frequency could also be optimized to decrease the losses. However, if the total losses of the drive system are considered, a compromise has to be made between the machine losses and the switching losses in the inverter, which grow with higher switching frequencies, contrary to the core losses of the machine.

References

[1] Z. Gmyrek, A. Boglietti, A. Cavagnino, "Iron Loss Prediction With PWM Supply Using Low- and High-Frequency Measurements: Analysis and Results Comparison," *IEEE Trans. Ind. Electr.*, Vol. 55, No. 4, pp. 1722-1728, April 2008.

[2] M. Popescu, D. M. Ionel, A. Boglietti, A. Cavagnino, C. Cossar, M. I. McGilp, "A General Model for Estimating the Laminated Steel Losses Under PWM Voltage Supply," *IEEE Trans. Ind. Appl.*, Vol. 46, No. 4, pp. 1389-1396, July/August 2010.

[3] N. Stranges, J. H. Dymond, "How Design Influences the Temperature Rise of Motors on Inverter Drives," *IEEE Trans. Ind. Appl.*, Vol. 39, No. 6, pp. 1584-1591, November/December 2003.

[4] A. Knight, Y. Zhan, "Identification of flux density harmonics and resulting iron losses in induction machines with nonsinusoidal supplies", *IEEE Trans. Magn.*, Vol. 44, No. 6, pp. 1562–1565, June 2008.

[5] R. Liu, C. C. Mi, D. W. Gao, "Modeling of Eddy-Current Losses of Electrical Machines and Transformers Operated by Pulsewidth-Modulated Inverters," *IEEE Trans. Magn.*, Vol. 44, No. 8, pp. 2021-2028, August 2008.

[6] E. Dlala, A. Arkkio, "A General Model for Investigating the Effects of the Frequency Converter on the Magnetic Iron Losses of a Squirrel-Cage Induction Motor," *IEEE Trans. Magn.*, Vol. 45, No.9, pp. 3303-3315, September 2009.

[7] Z. Gmyrek, A. Boglietti, A. Cavagnino, "Estimation of Iron Losses in Induction Motors: Calculation Method, Results, and Analysis," *IEEE Trans. Ind. Electr.*, Vol. 57, No. 1, pp. 161-171, January 2010.

[8] A. Boglietti, A. Cavagnino, M. Lazzari, "Fast Method for the Iron Loss Prediction in Inverter-Fed Induction Motors," *IEEE Trans. Ind. Appl.*, Vol. 46, No. 2, pp. 806-811, March/April 2010.

[9] A. Boglietti, A. Cavagnino, L. Ferrari, M. Lazzari, "Impact of the Supply Voltage on the Stray-Load Losses in Induction Machines," *IEEE Trans. Ind. Appl.*, Vol. 46, No. 4, pp. 1374-1380, July/August 2010.

[10] A. Boglietti, A. Cavagnino, D. M. Ionel, M. Popescu, D. A. Stanton, S. Vaschetto, "A General Model to Predict the Iron Losses in PWM Inverter-Fed Induction Motors," *IEEE Trans. Ind. Appl.*, Vol. 46, No. 5, pp. 1882-1890, September/October 2010.

[11] A. Knight, J. Salmon, J. Ewanchuk, "A Simple Method to Account for PWM Eddy Current Iron Losses in Finite Element Analysis," ECCE, Phoenix, AZ, USA, September 2011.

[12] Z. Gmyrek, A. Boglietti, A. Cavagnino, "No-Load Loss Separation in Induction Motors Operated by PWM Inverters: Numerical and Experimental Approaches," IECON, Melbourne, Australia, November 2011.

[13] L. Aarniovuori, L. I. E. Laurila, M. Niemelä, J. Pyrhönen, "Measurements and simulations of DTC voltage source converter and induction motor losses", *IEEE Trans. Ind. Electr.*, Vol. 59, No. 5, pp. 2277–2287, May 2012.

[14] Z. Nannan, Z. Q. Zhu, L. Weiguo, "Rotor Eddy Current Loss Calculation and Thermal Analysis of Permanent Magnet Motor and Generator," *IEEE Trans. Magn.*, Vol. 47, No. 10, pp. 4199-4202, October 2011.

[15] K. Yamazaki, Y. Fukushima, "Effect of Eddy-Current Loss Reduction by Magnet Segmentation in Synchronous Motors with Concentrated Windings," *IEEE Trans. Ind. Appl.*, Vol.47, No. 2, pp. 779-788, March/April 2011.

[16] C. P. Steinmetz, "On the Law of Hysteresis," *Am. Inst. Electr. Eng. Trans.*, Vol. 9, pp. 3-64, 1892, Reprinted in *Proc. IEEE*, Vol. 72, No. 2, pp. 197-221, February 1984.

[17] G. Bertotti, "General Properties of Power Losses in Soft Ferromagnetic Materials," *IEEE Trans. Magn.*, Vol. 24, No. 1, pp. 621-630, January 1988.

[18] W. Cao, K. J. Bradley, J. C. Clare, P. W. Wheeler, "Comparison of Stray Load and Inverter-Induced Harmonics Losses in Induction Motors Using Calorimetric and Harmonic Injection Methods," *IEEE Trans. Ind. Appl.*, Vol. 46, No. 1, pp. 249-255, January/February 2010.

[19] W. Vetter, K. Reichert, "Determination of damper winding and rotor iron currents in convertor- and line-fed synchronous machines," *IEEE Trans. Energy Convers*., Vol. 9, No. 4, pp. 709–716, December 1994.

[20] S. Shisha, C. Sadarangani, H.-P. Nee, "Loss distribution on solid pole plates of wound-rotor synchronous motors fed from inverters using direct torque control", *IEEE Trans. Energy Convers.*, Vol. 27 No. 1, pp. 63–70, March 2012.

[21] R. Emery, J. Eugene, "Harmonic losses in LCI-fed synchronous motors", *IEEE Trans. Ind. Appl.* Vol. 38, No. 4, pp. 948–954, July/August 2002.

[22] P. Beckley, N. J. Layland, E. Hopper, D. Power, "Impact of surface coating insulation on small motor performance," *IEE Proc. Electr. Power Appl.*, Vol. 145, No. 5, pp. 409-413, September 1998.

[23] E. Bjerkan, "High-Frequency Modeling of Power Transformers – Stresses and Diagnostics," Ph.D. thesis, Norwegian University of Science and Technology, Trondheim, Norway, 2005, available at http://ntnu.diva-portal.org/smash/get/diva2:125733/FULLTEXT01.

[24] A. Coombs, M. Lindenmo, D. Snell, D. Power, "Review of the Types, Properties, Advantages, and Latest Developments in Insulating Coatings on Nonoriented Electrical Steels," *IEEE Trans. Magn.*, Voo. 37, No. 1, pp. 544-557, January 2001.

[25] P. Rasilo, J. Ekström, A. Haavisto, A. Belahcen. A. Arkkio, "Calorimetric System for Measurement of Synchronous Machine Losses," *IET Electr. Power Appl.*, Vol. 6, No. 5, pp. 286-294, May 2012.

[26] P. Rasilo, E. Dlala, K. Fonteyn, J. Pippuri, A. Belahcen, A. Arkkio, "Model of Laminated Ferromagnetic Cores for Loss Prediction in Electrical Machines," *IET Electr. Power Appl.*, Vol. 5, No. 7, pp. 580-588, August 2011.

[27] P. Rasilo, A. Belahcen. A. Arkkio, "Importance of Iron Loss-Modeling in Simulation of Wound-Field Synchronous Machines," *IEEE Trans. Magn.*, Vol. 48, No. 9, pp. 2495-2504, September 2012.

[28] H. Karmaker, A. M. Knight, "Investigation and Simulation of Fields in Large Salient-Pole Synchronous Machines With Skewed Stator Slots," *IEEE Trans. Energy Convers.*, Vol. 20, No. 3, pp. 604-610, September 2005.

[29] A. M. Knight, S. Troitskaia, N. Stranges, A. Merkhouf, "Analysis of large synchronous machines with axial skew, part 1: flux density and open-circuit voltage harmonics," *IET Electr. Power Appl.*, Vol. 3, No. 5, pp. 389-397, September 2009.

[30] A. M. Knight, S. Troitskaia, N. Stranges, A. Merkhouf, "Analysis of large synchronous machines with axial skew, part 2: inter-bar resistance, skew and losses," *IET Electr. Power Appl.*, Vol. 3, No. 5, pp. 398-406, September 2009.

[31] S. Englebretson, “Induction Machine Stray Loss from Inter-Bar Currents,” Ph.D. thesis, Massachusetts Institute of Technology, 2009.

[32] Y. Zhan, A. M. Knight, N. Stranges, “Multislice Inter-Bar Model for Large Synchronous Machines With Skewed Stator Slots,” *IEEE Trans. Magn.*, Vol. 45, No.3, pp.1800-1803, March 2009.

[33] I. D. Mayergoyz, “Mathematical Models of Hysteresis (invited),” *IEEE Trans. Magn.*, Vol. MAG-22, No. 5, pp. 603-608, September 1986.

[34] F. C. F. Guerra, W. S. Mota, “Magnetic Core Model,” *IET Sci. Meas. Technol.*, Vol. 1 No. 3, pp. 145-151, May 2007.

[35] I. D. Mayergoyz, “Vector Preisach hysteresis models (invited),” *J. Appl. Phys.*, Vol. 63, No. 8, pp. 2995-3000, April 1988.

[36] L. Stoleriu, P. Andrei, A. Stancu, “First order reversal curves identification procedures for vector models of hysteresis,” *J. Appl. Phys.*, Vol. 103, No. 7, March 2008.

[37] P. Rasilo, A. Arkkio, “Modeling the Effect of Inverter Supply on Eddy-Current Losses on Synchronous Machines,” SPEEDAM, Pisa, Italy, June 2010.

[38] P. Rasilo, A. Belahcen, A. Arkkio, “Effect of Rotor Pole-Shoe Construction on Losses of Inverter-Fed Synchronous Motors,” ICEM, Marseilles, France, September 2012.

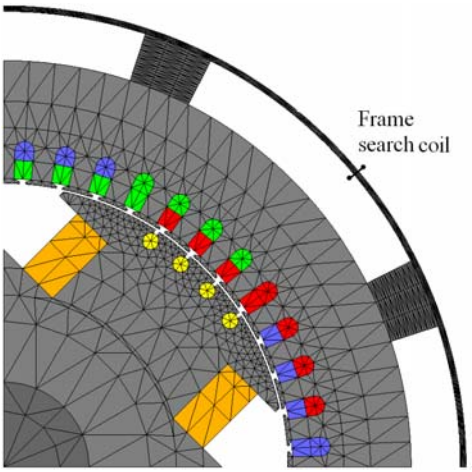

Fig. 1 Geometry and FE mesh of the studied machine.

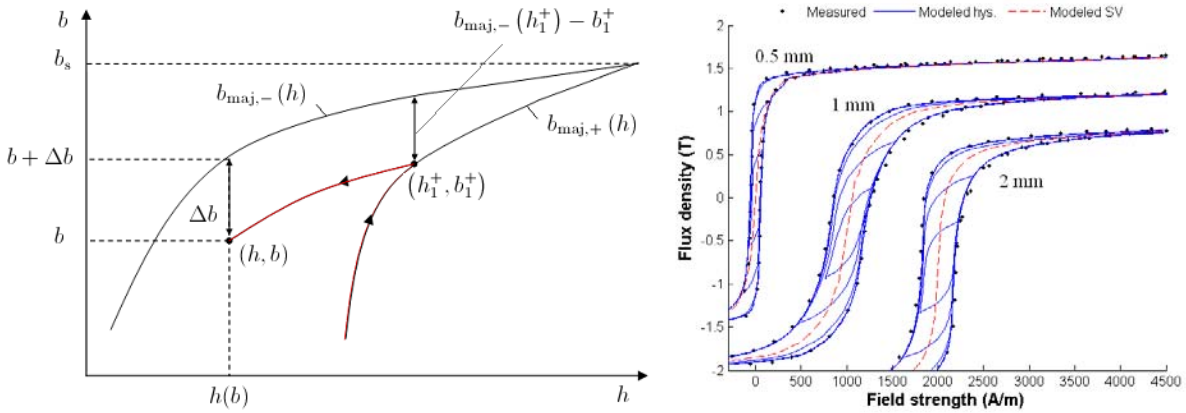

a) b)

Fig. 2 a) Notation in the analytical definition of the FORCs and b) measured and modeled magnetization properties for the three materials (the 1-mm and 2-mm ones are shifted from the origin for clarity).

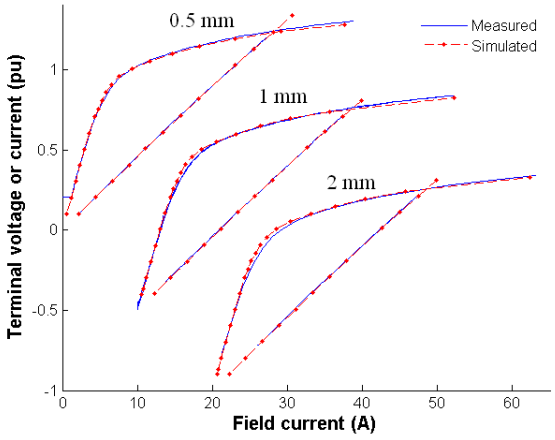

Fig. 3 Measured and simulated no-load and short-circuit curves for the machine with the three rotors (the 1-mm and 2-mm ones are shifted from the origin for clarity).

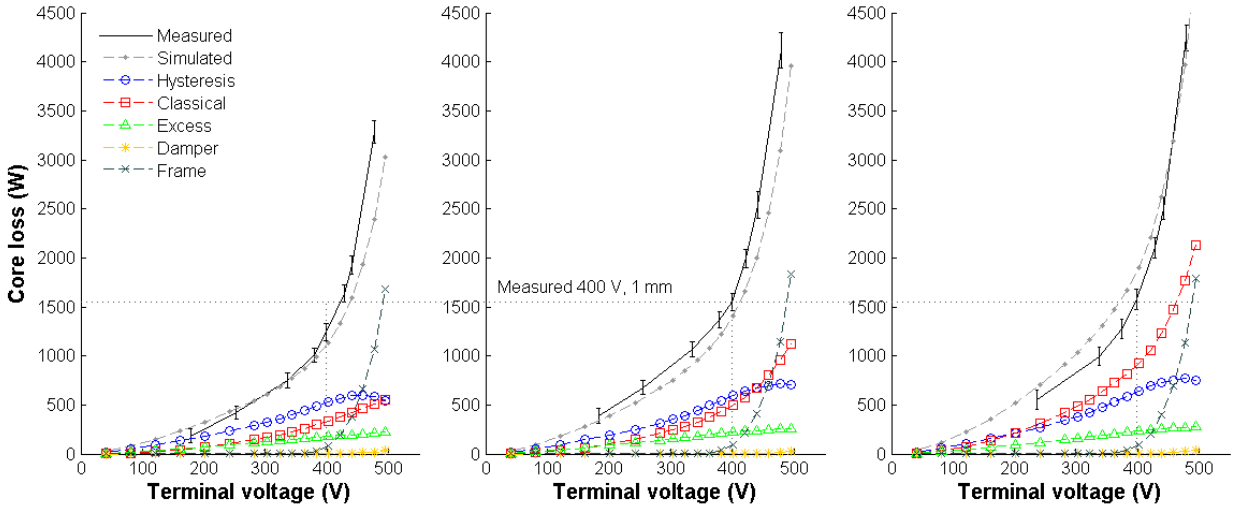

Fig. 4 Measured and simulated no-load core losses as a function of the terminal voltage.

a) 0.5-mm rotor, b) 1-mm rotor and c) 2-mm rotor.

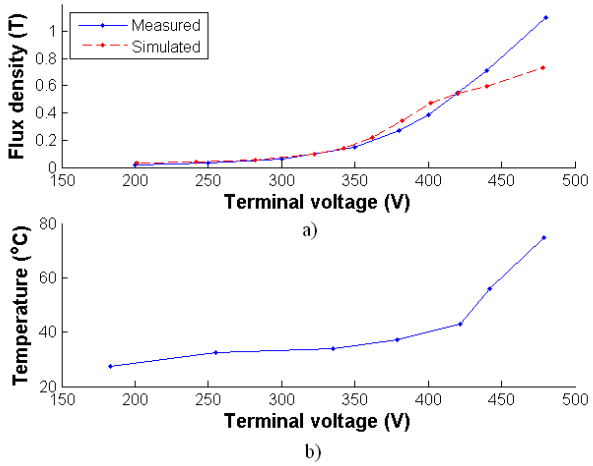

Fig. 5 a) Measured and simulated peak flux densities and b) the measured temperatures in the frame at no load with the 1-mm rotor.

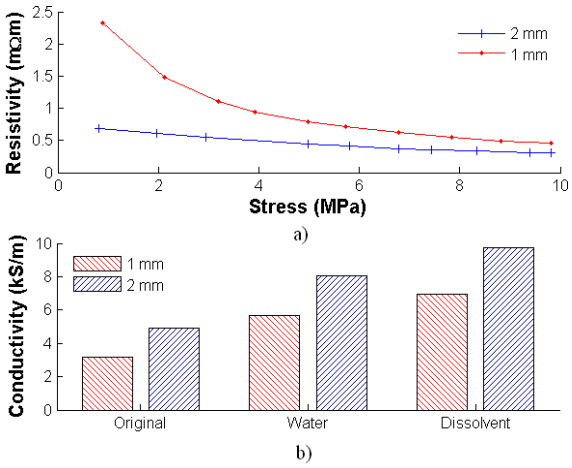

Fig. 6 a) Measured lamination stack axial resistivities as a function of pressing stress and b) increases in the conductivities as a result of cleansing.

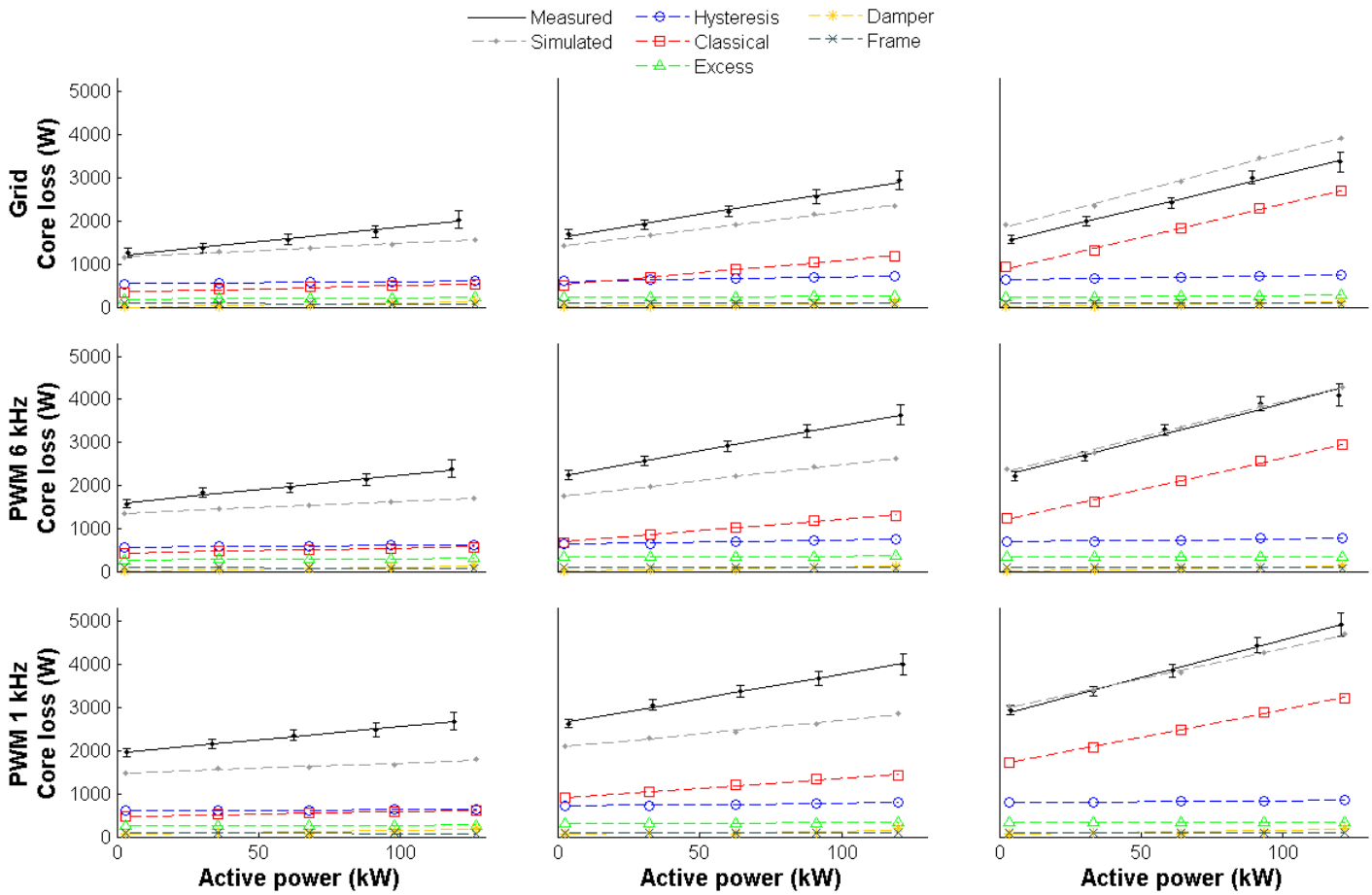

Fig. 7 Measured and simulated core losses as a function of load with grid supply and 6-kHz and 1-kHz PWM supplies. The lines are fitted to the results by leas-squares fitting. a) 0.5-mm rotor, b) 1-mm rotor and c) 2-mm rotor.

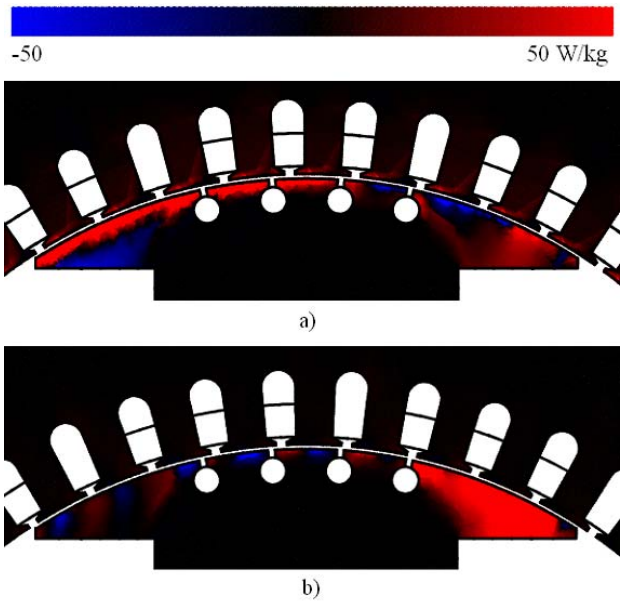

Fig. 8 Differences in the iron-loss distributions with the 1-mm rotor a) between the rated-load and no-load operation points in the 1-kHz PWM case and b) between the 1-kHz PWM supply and grid supply in the rated-load operation. Direction of rotation is counterclockwise.

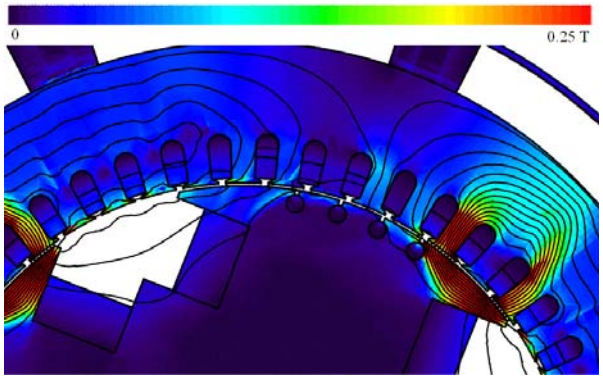

Fig. 9 Instantaneous high-frequency flux, i.e. the difference in the flux-density distribution between the 1-kHz PWM supply and grid supply in the machine with the 1-mm rotor. Direction of rotation is counterclockwise.

TABLE I
DATA AND DIMENSIONS OF THE MACHINE

Machine type	generator
Power	150 kVA
Voltage	400 V
Current	217 A
Displacement factor	0.8 cap
Frequency	50 Hz
Connection	star
Number of pole pairs	2
Stator outer diameter	430 mm
Stator inner diameter	300 mm
Air gap	1.2 mm
Number of stator slots	48

TABLE II
LAMINATION MATERIALS

Sheet	**Thickness (mm)**	**Conductivity (MS / m)**
Stator sheet / Rotor sheet 1	0.5	3.00
Rotor sheet 2	1	7.61
Rotor sheet 3	2	7.85

TABLE III
NUMERICAL VALUES OF THE MEASURED AND SIMULATED CORE LOSSES, ERROR LIMITS FOR THE FORMER AND SEGREGATION OF THE LATTER INTO STATOR AND ROTOR LOSSES

Core loss (W)		**0.5-mm rotor sheet**					**1-mm rotor sheet**					**2-mm rotor sheet**				
No-load voltage (V)		**250**	**335**	**400**	**440**	**480**	**250**	**335**	**400**	**440**	**480**	**250**	**335**	**400**	**440**	**480**
Open-circuit operation	**Meas.**	412 ± 69	747 ± 73	1257 ± 86	1913 ± 93	3437 ± 120	658 ± 69	1070 ± 75	1550 ± 84	2478 ± 128	4176 ± 175	636 ± 95	979 ± 96	1597 ± 100	2438 ± 108	4264 ± 130
	Sim, st.	407	668	1017	1467	2352	406	667	1023	1502	2455	407	669	1024	1501	2448
	Sim, rt.	44	69	99	125	162	140	244	365	504	740	333	582	848	1133	1662
Load (%)		**0**	**25**	**50**	**75**	**100**	**0**	**25**	**50**	**75**	**100**	**0**	**25**	**50**	**75**	**100**
Grid supply	**Meas.**	1237 ± 100	1363 ± 102	1562 ± 114	1742 ± 138	2019 ± 194	1664 ± 103	1894 ± 105	2210 ± 119	2541 ± 150	2935 ± 214	1493 ± 100	1979 ± 106	2400 ± 121	3009 ± 156	3354 ± 224
	Sim, st.	1038	1127	1193	1229	1239	1044	1145	1217	1272	1301	1043	1145	1214	1263	1289
	Sim, rt.	111	129	155	208	291	369	499	674	869	1047	834	1147	1619	2140	2607
6-kHz PWM supply	**Meas.**	1541 ± 100	1836 ± 106	1944 ± 117	2154 ± 146	2397 ± 204	2205 ± 106	2569 ± 112	2913 ± 127	3287 ± 160	3629 ± 224	2118 ± 103	2680 ± 111	3320 ± 131	3864 ± 166	4100 ± 248
	Sim, st.	1155	1233	1292	1326	1338	1149	1241	1311	1362	1391	1135	1229	1296	1344	1369
	Sim, rt.	188	199	224	277	353	599	706	870	1057	1247	1210	1496	1956	2463	2905
1-kHz PWM supply	**Meas.**	1929 ± 102	2121 ± 107	2328 ± 121	2468 ± 150	2684 ± 217	2563 ± 97	2998 ± 114	3317 ± 131	3649 ± 164	3972 ± 238	2863 ± 110	3317 ± 117	3822 ± 138	4406 ± 176	4896 ± 272
	Sim, st.	1181	1273	1318	1336	1347	1183	1288	1335	1372	1420	1168	1278	1325	1357	1388
	Sim, rt.	277	294	287	319	414	907	974	1081	1237	1431	1814	2079	2421	2852	3280